2011 IEEE/RSJ International Conference on
Intelligent Robots and Systems
September 25-30, 2011. San Francisco, CA, USA

Experiments of Passivity-Based Bilateral Aerial Teleoperation of a Group of UAVs with Decentralized Velocity Synchronization

Paolo Robuffo Giordano, Antonio Franchi, Cristian Secchi, and Heinrich H. Bülthoff

Abstract— **In this paper, we present an experimental validation of a novel decentralized passivity-based control strategy for teleoperating a group of Unmanned Aerial Vehicles (UAVs): the slave side, consisting of the UAVs, is endowed with large group autonomy by allowing time-varying topology and inter-robot/obstacle collision avoidance. The master side, represented by a human operator, controls the group motion and receives suitable force feedback cues informing her/him about the remote slave motion status. Passivity theory is exploited for guaranteeing stability of the slave side and of the overall teleoperation channel. Results of experiments involving the use of 4 quadcopters are reported and discussed, confirming the soundness of the paper theoretical claims.**

I. INTRODUCTION

Bilateral teleoperation of multiple robots is an emerging topic in the robotics community as reported in several previous works ranging from [1], [2] up to the more recent [3], [4], [5]. Indeed, on the one hand a group of simple (mobile) robots rather than a single complex robot has proven to be very effective in several applications such as surveillance, search and rescue, cooperative transportation and exploration of wide areas [6], [7]. On the other hand, because of the large complexity of these tasks, full robotic autonomy is still far from being reached, and some level of human intervention is required. Therefore, in many practical cases, the use of a semi-autonomous group of robots partially guided by a human operator still represents the only viable solution. In these situations, introducing a suitable sensorial feedback for the human operator, i.e., realizing a *bilateral* teleoperation channel, has also been confirmed to improve the human (tele-)presence, in particular by exploiting the haptic (force-feedback) sense [8], [9].

Among the various possibilities for providing mobility to a robot, the capability of *flying* is undoubtedly one of the most intriguing and explored over the last years: Unmanned Aerial Vehicles (UAVs) promise large flexibility and pervasiveness in many different scenarios, possessing a mobility potentially unrivalled by most other solutions [10]. It is then interesting to study the establishment of a bilateral teleoperation channel interfacing a human operator with a remote group of semi-autonomous UAVs — the so-called *Aerial Teleoperation*. In a recent work [4], we proposed a novel decentralized control strategy for teleoperating a group of UAVs: the emphasis was placed on rendering the behavior of the UAVs as flexible as possible, by ensuring inter-agent and obstacle collision avoidance, and by adapting online the formation shape and topology via local splitting and merging decisions. The human operator at the master side was feeling, through suitable force cues, the motion state of the fleet and the presence of (remote) obstacles. However, no synchronization among the UAVs actual velocities and the human/master velocity commands could be achieved because of a too conservative local damping action on the UAV side, and only hardware-in-the-loop simulations were reported.

In this respect, the goals of this paper are twofold: first, we extend the theory behind [4] in order to cope with the open points mentioned above, and second we rigorously characterize the teleoperation steady-state behavior, both in terms of slave motion and force reflection on the master side. In addition, we also provide an evaluation of the theoretical claims by reporting full experiments obtained with 4 quadcopters teleoperated by a human operator.

The rest of the paper is organized as follows: Sect. II briefly reviews the framework developed in [4] which also forms the basis of the current paper. Then, Sect. III introduces the theoretical contributions of this work by addressing the issues of master/slave velocity synchronization and steady-state characteristics, and Sects. IV–V illustrate the experimental setup and discuss the results of the experiments. Finally, Sect. VI concludes the paper and addresses future directions of our research.

II. REVIEW OF PASSIVE TELEOPERATION OF MULTIPLE UAVs WITH SWITCHING TOPOLOGY

In this Section, we will briefly summarize the theoretical framework introduced in [4] for teleoperating a group of UAVs in a decentralized way. We consider the slave side as a group of N agents that can be modeled as floating masses in $\mathbb{R}^3$ among which a *leader* is chosen. The motion of an agent depends on the motion of the surrounding agents and obstacles, while the leader is a special agent that is also controlled by the master. In order to consider the difference between the limited workspace of a master robot and the unbounded one of a UAV, teleoperation is made in the following sense: the position of the master device is treated as a velocity setpoint for the leader at the slave side, and the mismatch between the master position and the actual leader velocity is transformed into a force at the master side in order to transmit to the user a feeling of the remote side.

P. Robuffo Giordano and A. Franchi are with the Max Planck Institute for Biological Cybernetics, Spemannstraße 38, 72076 Tübingen, Germany {prg,antonio.franchi}@tuebingen.mpg.de.

C. Secchi is with the Department of Science and Methods of Engineering, University of Modena and Reggio Emilia, via G. Amendola 2, Morselli Building, 42122 Reggio Emilia, Italy cristian.secchi@unimore.it

H. H. Bülthoff is with the Max Planck Institute for Biological Cybernetics, Spemannstraße 38, 72076 Tübingen, Germany, and with the Department of Brain and Cognitive Engineering, Korea University, Anam-dong, Seongbuk-gu, Seoul, 136-713 Korea hhb@tuebingen.mpg.de.

978-1-61284-455-8/11/$26.00 ©2011 IEEE

A. The Master Side

We assume the master to be a generic mechanical system described by the following Euler-Lagrange equations:

$$M_M(x_M)\ddot{x}_M + C_M(x_M, \dot{x}_M)\dot{x}_M + D_M\dot{x}_M = F_M \quad (1)$$

where $M_M(x_M)$ represents the inertia matrix, $C(x_M, \dot{x}_M)\dot{x}_M$ is a term representing the centrifugal and Coriolis effects, and D_M is a matrix representing both the viscous friction present in the system and any additional damping injection via local control actions. We also assume that gravity is locally compensated. The variables x_M and $v_M := \dot{x}_M$ represent the position and the velocity of the end-effector. In [11], the authors showed how to render the master (1) passive w.r.t. the pair (F_M, r) with storage function $V_M = \frac{1}{2} r^T M_M r$ and $r = v_M + \lambda x_M$, $\lambda > 0$. This was obtained by a suitable pre-feedback action requiring knowledge of the matrixes M_M and C_M in (1). By introducing a scaling into this strategy, one can also render the master passive w.r.t. the scaled pair (F_M, r_M) where

$$r_M = \rho r = \rho v_M + \rho\lambda x_M, \qquad \rho > 0,\ \lambda > 0 \quad (2)$$

and new (scaled) storage function $\bar{V}_M = \rho V_M$. By properly choosing the design parameters ρ and λ, it is then possible to make negligible the contribution related to v_M (by choosing a small ρ), and to make the second term proportional to the position with a desired scaling factor K (by choosing $\lambda = \frac{K}{\rho}$). Therefore, one can exploit the position-like variable r_M in order to passively couple the master side with the remote slave side through the power port (F_M, r_M).

B. The Slave Side

1) Model of the Agents: The UAVs are assumed to be endowed with a Cartesian trajectory tracking controller (as, for instance, the one proposed in [12]) ensuring a closed loop behavior close enough to that of a fully actuated floating mass in $\mathbb{R}^3$. We then model each agent, and its local control structure, as:

$$\begin{cases} \dot{p}_i = F_i^{\mathrm{a}} + F_i^{\mathrm{e}} - B_i M_i^{-1} p_i \\ \dot{t}_i = (1-\beta_i)(\alpha_i \frac{1}{t_i} D_i + w_i) + \beta_i c_i \\ y_i = \begin{pmatrix} M_i^{-1} p_i \\ t_i \end{pmatrix} \end{cases} \qquad i = 1, \ldots, N \quad (3)$$

Here, $p_i \in \mathbb{R}^3$ and $M_i \in \mathbb{R}^{3\times 3}$ represent the momentum and the inertia matrix of agent i, respectively, $\mathcal{K}_i = \frac{1}{2} p_i^T M_i^{-1} p_i$ is the kinetic energy stored by the agent during its motion, and $B_i \in \mathbb{R}^{3\times 3}$ is a positive semidefinite matrix representing an artificial damping added for asymptotically stabilizing the behavior of the agent. Forces $F_i^{\mathrm{a}} \in \mathbb{R}^3$ and $F_i^{\mathrm{e}} \in \mathbb{R}^3$ represent the interaction of agent i with other agents and with the external world (i.e., the obstacles or the master side), respectively.

The power dissipated by the agents because of their local damping B_i, i.e.,

$$D_i = p_i^T {M_i^{-1}}^T B_i M_i^{-1} p_i, \quad (4)$$

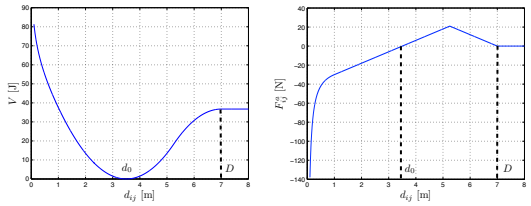

Fig. 1: The shape of the interagent potential as a function of the distance (left), and its corresponding coupling force (right).

is monitored and stored back into the local energy variable $T_i = \frac{1}{2} t_i^2 \in \mathbb{R}$ called *tank* [13], whose state $t_i \in \mathbb{R}$ augments the agent dynamics in Eq. (3). The quantities $\alpha_i, \beta_i \in \{0, 1\}$ in (3) are control parameters used to: *(i)* disable/enable the storage of D_i into the tank by activating α_i, and *(ii)* disable/enable a redistribution of the energy stored among the tanks of the N agents through the input c_i by activating β_i. Because of the reasons reported in [14], it is wise to disable the energy storage for avoiding an excess of energy stored that would potentially allow to implement practically unstable behaviors in the system. Thus, α_i is set to 0 if the energy stored in the tank reaches an upper bound $\bar{T}_i$ to be selected depending on the particular application. We also set a small threshold $\epsilon > 0$ below which energy extraction from the tank is prevented, in order to avoid singularities in (3).

The quantity $w_i \in \mathbb{R}$ in (3) is an additional input, exploited later on, used to exchange energy with the tank through the port (w_i, t_i). Finally, the outputs of the overall system (3) are the velocity of the agent $v_i = M_i^{-1} p_i$ and the tank state t_i. It is possible to prove that system (3) is passive w.r.t. its input/output ports, see [4].

2) Decentralized inter-agent interactions: Two agents are assumed to sense each other and to communicate (i.e., they are considered as *neighbors*) if their relative distance d_{ij} is less than $D \in \mathbb{R}^+$. Furthermore agents can measure the distance from any obstacle located within the range D. The agents are coupled so as to achieve a flexible, cohesive and collision free behavior by means of a set of interaction forces

$$F_i^{\mathrm{a}} = \sum_{j \neq i} F_{ij}^{\mathrm{a}}. \quad (5)$$

For each neighboring agent j, agent i computes an *inter-agent* interaction force F_{ij}^{a} whose magnitude and direction depends on the relative distance and bearing respectively. This force is designed so as to regulate the distance between the agents to a desired value d_0, to prevent collisions between the agents, and to vanish as the distance among the agents becomes larger than D. Figure 1 depicts the shape of a possible inter-agent force and associated scalar potential as a function of the inter-robot distance d_{ij}.

As explained in [4], such interaction force can be expressed as a nonlinear spring whose lower bounded potential energy function V depends on the relative position among the agents $x_{ij} := x_i - x_j \in \mathbb{R}^3$. Formally,

$$\begin{cases} \dot{x}_{ij} = v_{ij} \\ F_{ij}^{\mathrm{a}} = \frac{\partial V(x_{ij})}{\partial x_{ij}} \end{cases} \quad (6)$$

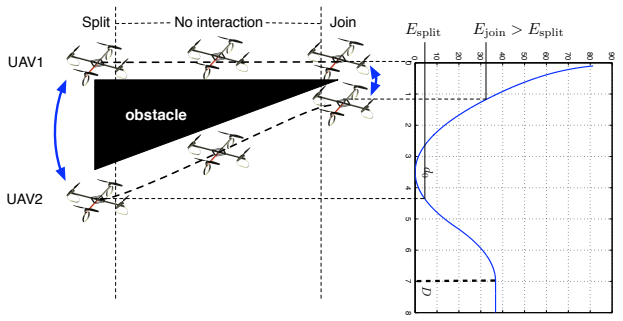

Fig. 2: When two agents split, the energy E_{split} is stored in the spring, while when they join the energy $E_{\text{join}} > E_{\text{split}}$ is needed to implement the new desired coupling. In this case, without proper strategies, an amount $E_{\text{join}} - E_{\text{split}} > 0$ of energy would be introduced into the system, thus violating passivity.

where $v_{ij} = v_i - v_j$ is the relative velocity among the agents. We note that the overall interaction force (5) can be computed in a decentralized way since, if agent j is not detected, i.e., it is not a neighbor, it is considered as being farther than D and a null force is implemented.

3) Split and Join Decisions: In order to enable the fleet to reshape its formation and/or to vary its topology in a flexible way, the agents are allowed to autonomously implement split and join decisions based on suitable strategies depending on the particular situation. We then refer to a *split* as the cancelation of the coupling force F^{a}_{ij} between a pair of agents i and j even though $d_{ij} \leq D$. A *join* is the (re-)establishment of the coupling, e.g., after a split. Clearly, a join can happen only if $d_{ij} \leq D$. Intuitively, a split between two agents mimics the disconnection from the virtual elastic element V_{ij} that represents their coupling. The spring becomes isolated and keeps on storing the same energy that was storing before the split decision, while the agents keep on interacting with the rest of the system. Thus, a split is a passivity preserving decision.

A join decision, on the other hand, can lead to a violation of passivity: when two agents i and j join, they instantaneously switch from a state characterized by no interaction, to the inter-agent interaction represented by Eq. (6). Some extra energy can be produced during the join procedure, possibly threatening the passivity of the system. In fact, in the general case, the relative distance of two agents at the join decision can be different from their relative distance at the split decision, and this can result in a non passive behavior: the illustrative example of Fig. 2 shows this situation.

To remedy this problem, we exploit the energy in the tanks T_i in order to passively implement join decisions that would otherwise violate the passivity constraint. In short, in the critical case of Fig. 2, agents i and j implement a join decision only if the sum of the energy stored in their tanks is greater than the energy produced by the (re-)establishment of the coupling. When this is not the case, the tanks are suitably recharged by either *(i)* exchanging energy with the tanks of the rest of the fleet (through the inputs c_i by setting $\beta_i = 1$ in Eq. (3)), or by *(ii)* increasing the local damping B_i until there is enough tank energy to passively implement the join decision. This procedure can be modeled as an exchange between the tanks and the nonlinear springs that couple the agents through the inputs w_i[1].

4) Passivity of the Overall Slave Side: Since the forces F^{a}_{ij} are symmetric, the interactions among the agents can be modeled as an undirected graph $\mathcal{G} = (\mathcal{V}, \mathcal{E})$ where the vertices represent the agents and an edge (i, j) represents the presence of a spring coupling agent i with agent j.

Defining $p = (p_1^T, \ldots, p_N^T)^T \in \mathbb{R}^{3N}$, $B = diag(B_i)$, $x = (x_{12}^T, \ldots, x_{1N}^T, x_{23}^T, \ldots, x_{2N}^T, \ldots, x_{N-1N}^T)^T \in \mathbb{R}^{3\frac{N(N-1)}{2}}$, $v = (v_1^T, \ldots, v_N^T)^T \in \mathbb{R}^{3N}$ and $F^e = (F_1^{eT}, \ldots, F_N^{eT})^T \in \mathbb{R}^{3N}$, the overall slave side (agents-tanks-springs) can be shown to take the compact form:

$$\begin{cases} \begin{pmatrix} \dot{p} \\ \dot{x} \\ \dot{t} \end{pmatrix} = \left[\begin{pmatrix} 0 & \mathcal{I} & 0 \\ -\mathcal{I}^T & 0 & \mathcal{I}_\gamma^T \\ 0 & -\mathcal{I}_\gamma & 0 \end{pmatrix} - \right. \\ \left. - \begin{pmatrix} B & 0 & 0 \\ 0 & 0 & 0 \\ -(I-\beta)\alpha PB & 0 & 0 \end{pmatrix} \right] \nabla H + \begin{pmatrix} 0 \\ 0 \\ \beta c \end{pmatrix} + GF^{\text{e}} \\ v = G^T \nabla H \end{cases} \tag{7}$$

where $\nabla H = \left(\frac{\partial^T H}{\partial p} \; \frac{\partial^T H}{\partial x} \; \frac{\partial^T H}{\partial t} \right)^T$ and

$$H = \sum_{i=1}^{N} \mathcal{K}_i + \sum_{i=1}^{N-1} \sum_{j=i+1}^{N} V(x_{ij}) + \sum_{i=1}^{N} T_i \tag{8}$$

represents the total energy of the overall slave side. Moreover, $\mathcal{I} = \mathcal{I}_\mathcal{G} \otimes I_3$, with $\mathcal{I}_\mathcal{G}$ being the incidence matrix of the graph $\mathcal{G}$ whose edge numbering is induced by the entries of the vector x. Matrix $G = \left((I_N \otimes I_3)^T \quad 0^T \right)^T$, with I_3 and I_N being the identity matrices of order 3 and N respectively, 0 represents a null matrix of proper dimensions, and $\otimes$ denotes the Krönecker product. The matrix $\mathcal{I}_\gamma = \Gamma \circ (\mathbf{1} \otimes \mathcal{I}_\mathcal{G})$, where $\circ$ is the element-wise product, $\mathbf{1} = \begin{pmatrix} 1 & 1 & 1 \end{pmatrix}^T$, and Γ is a matrix of proper dimensions whose elements represent an energetic interconnection between tanks and springs mediated by the inputs w_i in (3). Matrix P describes the storage of energy into the tanks and takes the expression

$$P = diag(\frac{1}{t_i} p_i^T M_i^{-T}) \quad i = 1, \ldots, N \tag{9}$$

Finally, $\alpha = diag(\alpha_i)$ and $\beta = diag(\beta_i)$ are matrices containing the mode switching parameters, $t = (t_1, \ldots, t_N)^T$, and $c = (c_1, \ldots, c_N)^T$. It is possible to show that that the system represented in Eq. (7) is passive with respect to the pair (F^e, v) using H as a storage function.

C. The Teleoperation System

Without loss of generality, suppose that agent 1 is chosen as the leader. It is possible to decompose $F_1^{\text{e}} = F_s + F_1^{\text{env}}$, where F_1^{env} is the component of the force due to the interaction with the external environment (obstacles) and F_s is the component due to the interaction with the master side. Similarly, we can decompose F_M in Eq. (1) as $F_M = F_m + F_h$, where F_h is the component due to the

[1]Full details of this strategy can be found in [4].

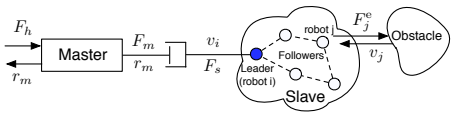

Fig. 3: The overall teleoperation system.

interaction with the user and F_m is the force acting on the master because of the interaction with the slave.

For achieving the desired teleoperation behavior, master and slave sides are joined using the following interconnection:

$$\begin{cases} F_s = -b_T(v_1 - r_M) \\ F_m = b_T(v_1 - r_M) \end{cases} \tag{10}$$

where $b_T > 0$ is a design parameter. This is equivalent to joining the master and the leader using a damper which generates a force proportional to the difference of the two velocity-like variables of the master and the leader. Since r_M is "almost" the position of the master, see Sect. II-A, the force fed back to the master and the control action sent to the leader are the desired ones. The complete teleoperation system, represented in Fig. 3, consists of the interconnection of a passive master side, a passive interconnection and a passive slave side. Recalling that the interconnection of passive systems is again passive, we can conclude that the teleoperation system is passive w.r.t. external actions (human force F_h and environment). We also note that, although not explicitly considered, passivity of the teleoperation system can be easily enforced also in presence of communication delays between local and remote sites using any of the techniques developed in conventional teleoperation settings as, e.g., wave variables [15].

III. DECENTRALIZED VELOCITY SYNCHRONIZATION

The approach proposed in [4] and reviewed in the previous Section allows to obtain a great flexibility of the fleet that can autonomously handle the navigation in cluttered environments. The agents can decide necessary split or join decisions without direct human intervention while preserving passivity of the overall teleoperation system. At the same time, the human operator can control the overall fleet motion by regulating the leader velocity through F_s in Eq. (10), and by receiving, through F_m, a force cue informative of the agent motion status.

Nevertheless, this control strategy for handling the group of agents can be too conservative. This is primarily due to the local damping action B_i, introduced in Eq. (3), which continuously dissipates energy: this energy replenishes the tank T_i until its maximum value $\bar{T}_i$ but is, otherwise, wasted. Furthermore, this continuous dissipation "brakes" the agents and prevents them from achieving velocity synchronization with the r_M variable of the master. Indeed, it can be proven that, at steady-state, the agents will synchronize to a fraction of the commanded r_M depending on the magnitude of their local damping B_i.

Therefore, the goal of this section is to modify the approach proposed in [4] for achieving velocity synchronization of the agents while still preserving the passivity of the overall controlled fleet, the interagent coupling and the possibility of passively implementing split and join decisions. We will also formally characterize the steady-state regimes of the coupled master/slave system in terms of achievable velocity synchronization and force reflection characteristics displayed to the human operator.

A. Variable Damping Action

We start by slightly modifying the structure of (3), modeling the agents as:

$$\begin{cases} \dot{p}_i = F_i^{\mathrm{a}} + F_i^{\mathrm{e}} + F_i^s + F_i^d \\ \dot{t}_i = (\frac{1}{t_i} D_i + w_i) \\ y_i = \begin{pmatrix} M_i^{-1} p_i \\ t_i \end{pmatrix} \end{cases} \quad i = 1, \ldots, N. \tag{11}$$

Here, the constant damping term B_i introduced in (3) has been replaced by a control action F_i^d defined as:

$$F_i^d = -B_i(t_i) M_i^{-1} p_i \tag{12}$$

where

$$B_i(t_i) = \begin{cases} 0 & \text{if} \quad T(t_i) = \bar{T}_i \\ \bar{B}_i & \text{if} \quad T(t_i) < \bar{T}_i \end{cases} \tag{13}$$

with $\bar{B}_i$ a positive definite matrix. The term F_i^d represents a variable damping action and, analogously to before, its associated dissipated power D_i is injected back into the tank T_i. However, this dissipation takes place only when a tank refill is necessary, as for example after an energy consuming join decision. This ensures that the tanks are timely refilled but avoids the dissipation of energy that could not be stored and which would constantly "brake" the agent. The control parameter α_i in (3) is not needed any longer because its role is played by the variable damping strategy in Eq. (13). Similarly, we also disregard the input c_i and the control parameter β_i.

Remark 1: Adopting (13) rather than the constant damping B_i in (3) allows to implement very 'large' damping actions only for very 'small' amounts of time in order to quickly refill the tanks. Indeed, for the sake of velocity synchronization and overall fleet behavior, a strong action but limited in time is more desirable than a small but persistent action.

Remark 2: The amount of energy that can be stored in the tank is bounded by the kinetic energy of the agent. If the agent stops before the tank is refilled, some join decicions may be temporarily forbidden because of lack of tank energy. Nevertheless, it is sufficient that the user starts acting on the system again for refilling the tank and restoring the normal situation.

The additional control action F_i^s in (11) is designed in order to synchronize the velocity of the agents

$$F_i^{\mathrm{s}} = -b \sum_{j \in \mathcal{N}_i} (v_i - v_j) \tag{14}$$

where $\mathcal{N}_i$ indicates the set of neighbors of agent i and $b > 0$ is a design parameter. This action is physically equivalent to a damper between neighboring agents. Since also this force is agent-wise symmetric, the interactions among the agents can

still be modeled by the same undirected graph $\mathcal{G} = (\mathcal{V}, \mathcal{E})$ exploited for the inter-agent couplings (6). Thus, a vertex in $\mathcal{G}$ will represent an agent and an edge (i, j) will represent the presence of a spring and of a damper among agents i and j. Considering Eq. (7), Eq. (11), Eq. (12), and Eq. (14), the new dynamics of the slave side becomes:

$$\begin{cases} \begin{pmatrix} \dot{p} \\ \dot{x} \\ \dot{t} \end{pmatrix} = \left[\begin{pmatrix} 0 & \mathcal{I} & 0 \\ -\mathcal{I}^T & 0 & \mathcal{I}_\gamma \\ 0 & -\mathcal{I}_\gamma^T & 0 \end{pmatrix} - \begin{pmatrix} \mathcal{L}+B & 0 & 0 \\ 0 & 0 & 0 \\ -PB & 0 & 0 \end{pmatrix} \right] \nabla H + GF^e \\ v = G^T \nabla H \end{cases} \tag{15}$$

with now B representing the block diagonal matrix whose elements are the variable dampers of Eq. (13). The matrix $\mathcal{L} = bL_\mathcal{G} \otimes I_3$, where $L_\mathcal{G}$ is the positive semidefinite Laplacian matrix of the graph $\mathcal{G}$, derives from the control action reported in Eq. (14), which is formally equivalent to a consensus algorithm among velocities (see, e.g., [16]), and H is the same lower bounded energy function given in Eq. (8).

Proposition 1: The slave side described in Eq. (15) is passive with respect to the pair of variables (F^e, v) and the storage function reported in Eq. (8).

Proof: From Eq. (15) it follows that:

$$\dot{H} = \nabla H^T \begin{pmatrix} \dot{p} \\ \dot{x} \\ \dot{t} \end{pmatrix} = -\frac{\partial^T H}{\partial p}(\mathcal{L}+B)\frac{\partial H}{\partial p} + \frac{\partial^T H}{\partial t} PB \frac{\partial H}{\partial p} + v^T F^e \tag{16}$$

Equation (9) implies that

$$\frac{\partial^T H}{\partial t} PB \frac{\partial H}{\partial p} = \frac{\partial^T H}{\partial p} B \frac{\partial H}{\partial p}$$

and therefore

$$\dot{H} = -\frac{\partial^T H}{\partial p}\mathcal{L}\frac{\partial H}{\partial p} + v^T F^e \leq v^T F^e \tag{17}$$

where the last inequality comes from the fact that $\mathcal{L}$ is positive semidefinite. This proves that the system represented in Eq. (15) is passive. ∎

Since the slave side with the new control strategy is still passive, joining the fleet to the modified master described in Sec. II-A by the interconnection proposed in Eq. (10) still yields a passive teleoperation system characterized by a stable behavior during interaction with the environment and human side.

B. Steady-state Behavior

In order to characterize the steady state behavior of the teleoperation system, we consider the external force acting on agent 1, the leader, split as $F_1^e = F_1^{env} + F_s$ where F_s is the master/slave coupling force of Eq. (10). The following result characterizes the behavior of the system in *free motion*.

Proposition 2: Let the master be kept at a constant configuration $(x_M, \dot{x}_M) \equiv (\bar{x}, 0)$ by a suitable human force F_h whose steady-state value will be determined in the following. Suppose also that (i) $F_i^e = 0$ for $i = 2, \ldots, N$ and $F_1^{env} = 0$ (agents moving in free motion), (ii) $B_i(t_i) = 0$ and $\mathcal{I}_\gamma = 0$ (tanks are full and no energy exchange takes place between tanks and springs), and (iii) the graph $\mathcal{G}$ is connected. Then, at steady-state:

1) the velocities of the agents synchronize to $K\bar{x}$;
2) the relative positions among the agents remain constant;
3) no force must be provided by the user, i.e., $F_h = 0$.

Proof: Apply the change of coordinates $\tilde{p}_i = p_i - M_i r_M$ and consider

$$\tilde{\mathcal{K}}_i = \frac{1}{2}\tilde{p}_i^T M_i^{-1} \tilde{p}_i, \quad \tilde{H} = \sum_{i=1}^{N} \tilde{\mathcal{K}}_i + \sum_{i=1}^{N-1} \sum_{j=i+1}^{N} V(x_{ij}) + \sum_{i=1}^{N} T_i,$$

as the 'new' kinetic and total energy of the slave side. Note also that, because of its definition, it is

$$\frac{\partial \tilde{H}}{\partial \tilde{p}} = v - \mathbf{1}_{N_3} r_M \tag{18}$$

where $\mathbf{1}_{N_3} = \mathbf{1}_N \otimes I_3$ and $\mathbf{1}_N \in \mathbb{R}^N$ is a column vector of all ones. Therefore, because of assumption (ii) and owing to the fact that $\mathcal{L}\mathbf{1}_{N_3} = 0$, $\mathcal{I}^T \mathbf{1}_{N_3} = 0$, and $\dot{\tilde{p}} = \dot{p}$ since $\dot{r}_M = K\dot{x}_M + \rho\ddot{x}_M \equiv 0$ (master kept fixed), the slave dynamics takes the form

$$\begin{cases} \begin{pmatrix} \dot{\tilde{p}} \\ \dot{x} \\ \dot{t} \end{pmatrix} = \left[\begin{pmatrix} 0 & \mathcal{I} & 0 \\ -\mathcal{I}^T & 0 & 0 \\ 0 & 0 & 0 \end{pmatrix} - \begin{pmatrix} \mathcal{L} & 0 & 0 \\ 0 & 0 & 0 \\ 0 & 0 & 0 \end{pmatrix} \right] \nabla \tilde{H} + GF^e \\ v = G^T \nabla \tilde{H} \end{cases} . \tag{19}$$

By exploiting assumption (i) and (10), we obtain

$$\dot{\tilde{H}} = -\frac{\partial^T \tilde{H}}{\partial \tilde{p}}\mathcal{L}\frac{\partial \tilde{H}}{\partial \tilde{p}} + \frac{\partial^T \tilde{H}}{\partial \tilde{p}_1} F_s = -\frac{\partial^T \tilde{H}}{\partial \tilde{p}}\mathcal{L}\frac{\partial \tilde{H}}{\partial \tilde{p}} - \frac{\partial^T \tilde{H}}{\partial \tilde{p}_1} b_T \frac{\partial \tilde{H}}{\partial \tilde{p}_1} \leq 0. \tag{20}$$

This shows that the state trajectories are bounded as the (positive definite) energy function $\tilde{H}$ is non-increasing over time. Furthermore, consider the set $S = \{(\tilde{p}, x, t) \mid \dot{\tilde{H}} = 0\}$: the trajectories belonging to this set must satisfy $\frac{\partial \tilde{H}}{\partial \tilde{p}_1} = 0$ and $\frac{\partial \tilde{H}}{\partial \tilde{p}} \in \mathcal{N}(\mathcal{L})$. From assumption (iii), it is well-known that $\mathrm{rank}(\mathcal{L}) = 3N - 3$ and $\mathcal{N}(\mathcal{L}) = \mathbf{1}_{N_3}$, implying that $\frac{\partial \tilde{H}}{\partial \tilde{p}} = 0$. Therefore, $S = \{(\tilde{p}, x, t) \mid \frac{\partial \tilde{H}}{\partial \tilde{p}} = 0\}$. From (19), this further implies $\dot{x} = 0$, while $\dot{\tilde{p}} = 0$ is implied by the constraint $\frac{\partial \tilde{H}}{\partial \tilde{p}} = 0$ which can hold iff $\tilde{p} \equiv 0$. Since $\dot{t} = 0$ follows from assumption (ii), we can conclude, by resorting to LaSalle's arguments on the set S, that the slave system (19) will converge towards the steady-state condition $(\dot{\tilde{p}}, \dot{x}, \dot{t}) = (0, 0, 0)$ with $\frac{\partial \tilde{H}}{\partial \tilde{p}} = 0$ resulting in:

1) synchronization of the slave velocities with $r_M = Kx_M = K\bar{x}$, as $\frac{\partial \tilde{H}}{\partial \tilde{p}} = 0 \Rightarrow v = \mathbf{1}_{N_3} r_M$ from (18);
2) constant inter-agent positions, as $\dot{x} = 0$;
3) null force applied by the human operator. Indeed, at steady-state, the master dynamics (1) reduce to $0 = F_m + F_h = b_T(v_1 - r_M) + F_h = F_h$.

∎

Remark 3: During a normal operation, the human user will be asked to apply a non-null force because of the mismatch between the commanded r_M and v_1. However, as shown above, this force cue will eventually vanish at steady-state informing her/him about the reached velocity synchronization among the agents.

Remark 4: Assumption (iii) requires a connected graph $\mathcal{G}$. However, the proof directly extends to the non-connected

case by replacing $\mathcal{G}$ with its connected component $\mathcal{G}'$ inclusive of the leader agent. In order to prevent dangerous situations, the agents not belonging to $\mathcal{G}'$ will implement a constat local damping B_{max} in place of (13) to quickly stop their motion and wait for a rejoin with $\mathcal{G}'$. This can be done by using a distributed procedure (e.g., the classic flooding algorithm [17]).

We now focus on an opposite steady-state condition involving a slave in a *hard contact* situation, i.e., with the agents obstructed by the environment (obstacles). We will again characterize the resulting force cue displayed to the human user.

Proposition 3: Let the master be kept at a constant configuration $(x_M, \dot{x}_M) \equiv (\bar{x}, 0)$ by a suitable human force F_h whose steady-state value will be determined in the following. Suppose also that (i) there exist suitable environmental forces F_i^e, for $i = 2 \dots N$, and F_1^{env} that keep $p \equiv v \equiv 0$ for all agents despite the human command (hard contact with the environment), and (ii) $\mathcal{I}_\gamma = 0$ (no energy exchange takes place between tanks and springs). Then, at steady-state:

1) the relative positions among the agents remain constant;
2) the force provided by the human operator is $F_h = -F_1^{env} - \sum_{i=2}^{N} F_i^e$ (static reflection of the environmental forces).

Proof: With reference to system (15), the condition $p \equiv 0$ implies $\frac{\partial H}{\partial p} \equiv 0$ which, in turn, yields $\dot{x} = 0$ and $\dot{t} = 0$ because of assumption (ii). Furthermore, expanding the first row of (15), we get

$$0 = \dot{p} = \mathcal{I}\frac{\partial H}{\partial x} - (\mathcal{L} + B)\frac{\partial H}{\partial p} + F^e = \mathcal{I}\frac{\partial H}{\partial x} + F^e. \quad (21)$$

By premultiplying (21) with $\mathbf{1}_{N_3}^T$ we have that

$$0 = \mathbf{1}_{N_3}^T \mathcal{I}\frac{\partial H}{\partial x} + \mathbf{1}_{N_3}^T F^e = \mathbf{1}_{N_3}^T F^e \quad (22)$$

which can be rewritten as

$$F_s = -F_1^{env} - \sum_{i=2}^{N} F_i^e.$$

As before, since the master is kept at a constant position by the user, (1) reduces to

$$0 = F_h + F_m = F_h - F_s = F_h + F_1^{env} + \sum_{i=2}^{N} F_i^e, \quad (23)$$

resulting in

1) constant inter-agent positions, as $\dot{x} = 0$;
2) exact static reflection of the environmental forces, as $F_h = -F_1^{env} - \sum_{i=2}^{N} F_i^e$ from (23).

■

IV. EXPERIMENTAL SETUP

A picture representing our experimental setup is shown in Fig 4. The master side consists of a 3-DOF force-feedback device, the Omega.3[2] (Fig. 4a), controlled via usb by a C++ program running on a dedicated GNU-Linux machine. This includes two threads: the first thread runs a synchronous loop at 2.5 KHz which accesses the current master position/velocity and sets the desired force F_m in (10). The second thread, running at a slower rate (125 Hz), acts as a network interface with the leader agent by exchanging the leader speed v_1 and the master command r_M.

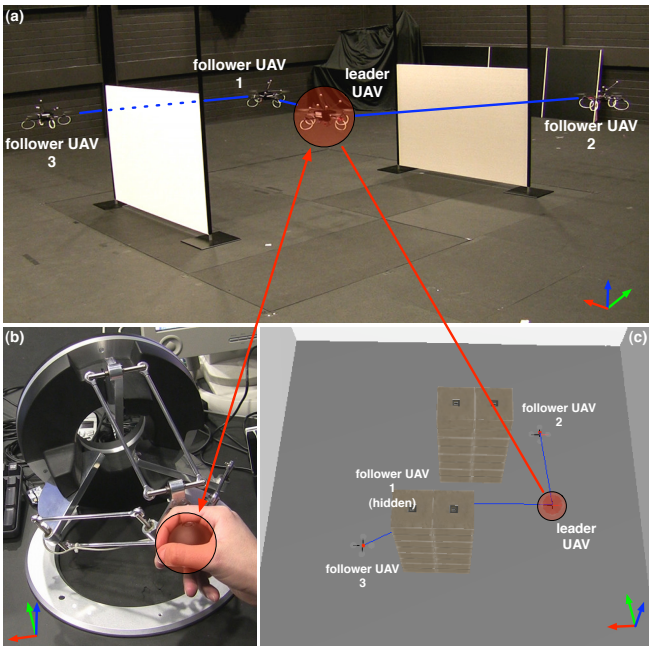

Fig. 4: The experimental setup.

The slave side is composed of 4 quadcopters[3] equipped with an embedded ATmega microprocessor and a standard integrated IMU (Fig. 4b). The microprocessor implements a low-level PID attitude controller by estimating the current attitude from the IMU measurements (via a complementary filter), and by controlling the pitch, roll, thrust and yaw-rate dofs of the UAV. This PID controller runs at about 450 Hz. Every quadcopter is also equipped with an additional Qseven single-board GNU-Linux machine[4] running a C++ program which implements a higher-level cartesian-control module: this computes the desired attitude and thrust commands and sends them to the low-level microprocessor via a serial interface whose baud rate is set to 115200. The Qseven board is also in charge of (1) communicating with the other UAVs via wireless ethernet, (2) communicating with the master device via wireless ethernet (only for the leader case), (3) implementing the inter-agent behavior described in Sects. II–III, and (4) retrieving the current UAV position (and numerically estimating its velocity) from an external tracking system — the VICON system[5]. All the ethernet communication is implemented with the UDP protocol.

Finally, the detection of obstacles in the environment is simulated by means of a custom-made simulation environment based on the OGRE3D[6] engine (Fig. 4c). This runs on a

[2] http://www.forcedimension.com

[3] http://www.mikrokopter.com

[4] http://www.seco.it

[5] http://www.vicon.com

[6] http://www.ogre3d.org/

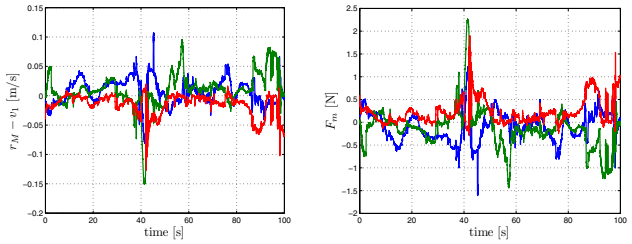

(a) (b)

Fig. 5: Results of the first experiment. Left: error between the commanded velocity r_M and the leader velocity v_1. Right: the force $F_m(t)$ displayed to the human operator on the master side.

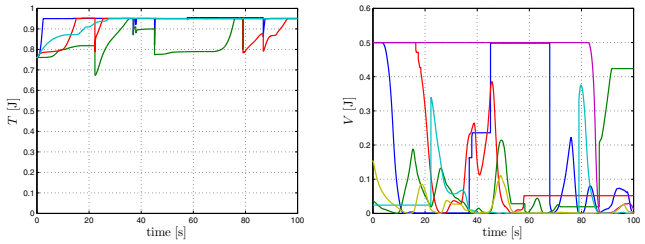

(a) (b)

Fig. 6: Results of the first experiment. Left: behavior of the 4 tank energies $T_i(t)$ over time. Right: behavior of the 6 link potentials $V_{ij}(t)$ over time. Note how (i) the tanks are constantly refilled during the experiment drawing from the energy dissipated by the local damping action (13), and (ii) how the tanks are instantaneously discharged when critical positive jumps in some of the $V_{ij}(t)$ occur.

separated machine connected to the same ethernet network of the UAVs from which it receives the corresponding (tracked) positions, and to which it sends back the surrounding obstacle points.

V. EXPERIMENTS

In this section we report the results of two experiments aimed at validating the proposed theoretical framework. The criterium adopted to decide a split between agents (see Sect. II-B) is visibility: two agents decide to split if their line-of-sight is obstructed by an obstacle, thus simulating the possible loss of visual/radio connectivity. We used the following numerical values for the various parameters appearing in the previous sections: $d_0 = 3$ [m] and $D = 5$ [m] for the inter-distance potential function of Fig. 1, $\rho = 0.01$ and $K = 6$ [s^{-1}] in (1), $b_T = 15$ [Ns/m] in (10), $\bar{B}_i = diag(5)$ [Ns/m] and $\bar{T} = 0.95$ [J] in (13), and $b = 0.4$ [Ns/m] in (14).

The first experiment consists of a number of maneuvers in the two-obstacle environment shown in Fig. 4a, and which can also be appreciated in the videoclip accompanying the paper. During this experiment, the human commands an overall slave motion that leads to several split and rejoin decisions, triggering in some cases the tank/spring energy exchange needed to preserve passivity of the slave side. Figure 5a reports the behavior of $r_M(t) - v_1(t)$ over time, i.e., the velocity discrepancy between master commands and leader velocity. It is possible to appreciate the close match among v_1 and r_M, indicating a good tracking performance. The force cue F_m displayed to the human operator during the experiment is shown in Fig. 5b: one can see that, as expected, the peaks of F_m occur during the transient discrepancies between r_M and v_1. These inform the human operator about the 'lag' between the leader agent and the master command: obstacle repulsions and/or presence of local damping $\bar{B}_i$ in (13) are the main sources of such discrepancies.

Figures 6a–6b show the evolution of the 4 tanks energies $T_i(t)$ and of the 6 inter-agent potentials V_{ij} (links) over time, with $V_{ij}(D) = 0.5$ [J]. At the beginning of the motion, 3 links start not connected with their potential at the 'infinity' value $V_{ij}(D)$ while, as time goes on, new links are created/destroyed as can be seen from the various jumps in the inter-agent potentials. Accordingly, the tank energies T_i in Fig. 6a start storing the energy dissipated by the local damping (13) until the maximum value $\bar{T}$ is reached and, at

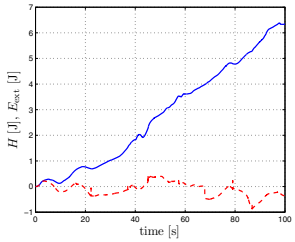

Fig. 7: Results of the first experiment. Behavior of $E_{\text{ext}}(t)$, the external energy supplied to slave system (solid blue line), and $E_{\text{in}}(t)$ the internal slave energy (dashed red line). Since $E_{\text{in}}(t) \leq E_{\text{ext}}(t)$, the passivity condition (17) of the slave system is confirmed.

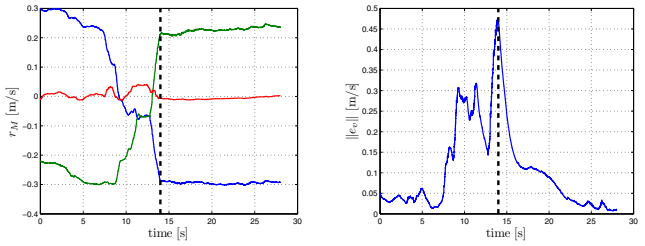

(a) (b)

Fig. 8: Results of the second experiment. Left: behavior of the master commands $r_M(t)$ over time. Right: behavior of $\|e_v(t)\|$, the norm of the velocity error of every agent w.r.t. the command r_M. The master commands are kept practically constant from about $t_1 = 14$ [s] until about $t_2 = 28$ [s], allowing for the velocity synchronization of the agent velocities.

the same time, get instantaneously discharged when critical (passivity-violating) positive jumps occur in some of the V_{ij} (see again Fig. 2). For instance, this happens at about times $t_1 = 22$ [s], $t_2 = 37$ [s], $t_3 = 45$ [s], $t_4 = 79$ [s], and $t_5 = 86$ [s]. Finally, from (17), Fig. 7 shows the superimposition of the external energy supplied to the slave system $E_{\text{ext}}(t) = \int_{t_0}^{t} v^T(\tau) F^e(\tau) \mathrm{d}\tau$ (blue solid line) and the variation of the internal slave energy $E_{\text{in}}(t) = H(t) - H(t_0)$ (red dashed line). From this plot, it is possible to verify that the passivity condition for the slave side (17) is always met as $E_{\text{in}}(t) \leq E_{\text{ext}}(t)$, $\forall t \geq t_0$.

The second experiment we report here is meant to illustrate the steady-state velocity synchronization and force cue

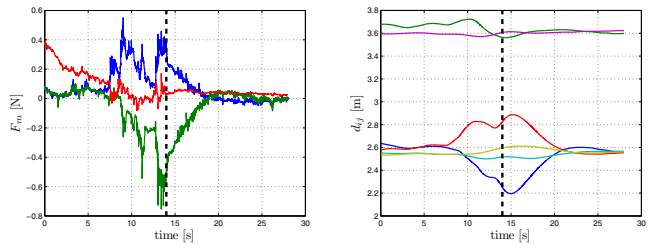

(a) (b)

Fig. 9: Results of the second experiment. Left: behavior of the master force F_m displayed to the human operator. Right: behavior of the agent interdistances d_{ij}. As $\|e_v(t)\| \to 0$ (indicating achievement of the velocity synchronization), $F_m \to 0$ and $d_{ij} \to const$ as discussed in Proposition 2.

behaviors discussed in Sect. III-B. To this end, we consider a flight phase during which the master commands are kept constant over a certain period of time in order to allow for the synchronization. Figure 8a shows the behavior of r_M: after about 14 [s], the master commands stay practically constant for about 30 [s]. During this phase, whose beginning is indicated by a dashed vertical line in the plots, the tanks are fully charged and no split/join decisions take place. In order to quantify the amount of velocity synchronization with the master command, we show in Fig. 8b the norm of $e_v = v - \mathbf{1}_{N_3} r_M$, i.e., the velocity error of the overall slave side w.r.t. r_M. It is possible to note that $\|e_v\|$ approaches 0 as the master commands stay constant, thus indicating the achievement of synchronization between all the v_i and r_M. Additionally, the master force F_m, shown Fig. 9a, vanishes during the same phase because of the reached synchronization. Since during this phase it is $F_m + F_h = 0$ as the master is kept fixed, it follows that $F_h \to 0$ confirming the conclusions drawn in Proposition 2 (null force applied by the human operator). Finally, we also report in Fig. 9b the behavior of the interdistances d_{ij} which become eventually constant as expected from Proposition 2.

VI. CONCLUSIONS AND FUTURE WORK

In this paper, we have presented an experimental validation of a decentralized control strategy based on passivity for teleoperating a groups of UAVs. The UAV motion and group topology is constrained as less as possible by allowing changes in shape and autonomous split/join decisions. By a proper passification of the master and slave sides, a bilateral teleoperation system coupling master commands with the UAV motion has been proposed, and a rigorous analysis of the steady-state performance in terms of achievable master/slave velocity synchronization and of force reflection characteristics was also discussed. Finally, we reported the successful results of real experiments obtained with 4 quadcopters teleoperated by a human user.

We are currently planning to rigorously analyze the effects of time delays on the stability of the proposed teleoperation system by both considering delays in the master/slave communication channel and delays among agents within the slave side.

ACKNOWLEDGEMENTS

This research was partly supported by WCU (World Class University) program funded by the Ministry of Education, Science and Technology through the National Research Foundation of Korea (R31-10008). The authors wish also to thank Johannes Lächele for his support on the development of the OGRE3D simulation environment.

REFERENCES

[1] S. Sirouspour, "Modeling and control of cooperative teleoperation systems," *IEEE Trans. on Robotics*, vol. 21, no. 6, pp. 1220–1225, 2005.

[2] E. J. Rodríguez-Seda, J. J. Troy, C. A. Erignac, P. Murray, D. M. Stipanović, and M. W. Spong, "Bilateral teleoperation of multiple mobile agents: Coordinated motion and collision avoidance," *IEEE Trans. on Control Systems Technology*, vol. 18, no. 4, pp. 984–992, 2010.

[3] D. J. Lee, A. Franchi, P. Robuffo Giordano, H. I. Son, , and H. H. Bülthoff, "Semi-Autonomous Haptic Teleoperation of Multiple Unmanned Aerial Vehicles over the Internet," in *2011 IEEE Int. Conf. on Robotics and Automation*, Shanghai, China, May 2011.

[4] A. Franchi, P. Robuffo Giordano, C. Secchi, H. Son, and H. Buelthoff, "A passivity-based decentralized approach for the bilateral teleoperation of a group of UAVs with switching topology," in *Proceedings of the 2011 IEEE International Conference on Robotics and Automation*, Shanghai, China, 2011.

[5] P. Robuffo Giordano, A. Franchi, C. Secchi, and H. H. Bülthoff, "Bilateral teleoperation of groups of UAVs with decentralized connectivity maintenance," in *Proceedings of the 2011 Robotics: Science and Systems Conference*, Los Angeles, USA, 2011.

[6] A. Howard, L. E. Parker, and G. S. Sukhatme, "Experiments with a large heterogeneous mobile robot team: Exploration, mapping, deployment and detection," *Intern. Journal of Robotics Research*, vol. 25, no. 5-6, pp. 431–447, 2006.

[7] J. Fink, N. Michael, S. Kim, and V. Kumar, "Planning and control for cooperative manipulation and transportation with aerial robots," *Intern. Journal of Robotics Research*, vol. 30, no. 3, 2010.

[8] B. Hannaford, L. Wood, D. McAffee, and H. Zak, "Performance evaluation of a six-axis generalized force-reflecting teleoperator," *Systems, Man and Cybernetics, IEEE Transactions on*, vol. 21, no. 3, pp. 620 –633, may/jun 1991.

[9] T. M. Lam, H. W. Boschloo, M. Mulder, and M. M. V. Paassen, "Artificial force field for haptic feedback in UAV teleoperation," *IEEE Transactions on Systems, Man, and Cybernetics, Part A: Systems and Humans*, vol. 39, no. 6, 2009.

[10] S. Bouabdallah, M. Becker, and R. Siegwart, "Autonomous miniature flying robots: Coming soon!" *IEEE Robotics and Automation Magazine*, vol. 13, no. 3, September 2007.

[11] N. Chopra, M. Spong, and R. Lozano, "Synchronization of bilateral teleoperators with time delay," *Automatica*, vol. 44, pp. 2142–2148, 2008.

[12] M.-D. Hua, T. Hamel, P. Morin, and C. Samson, "A Control Approach for Thrust-Propelled Underactuated Vehicles and its Application to VTOL Drones," *IEEE Trans. on Automatic Control*, vol. 54, no. 8, pp. 1837–1853, 2009.

[13] C. Secchi, S. Stramigioli, and C. Fantuzzi, "Position drift compensation in port-hamiltonian based telemanipulation," in *2006 IEEE/RSJ Int. Conf. on Intelligent Robots and Systems*, Beijing, China, Oct. 2006, pp. 4211–4216.

[14] D. J. Lee and K. Huang, "Passive-set-position-modulation framework for interactive robotic systems," *IEEE Trans. on Robotics*, vol. 26, no. 2, pp. 354–369, 2010.

[15] G. Niemeyer and J.-J. Slotine, "Telemanipulation with time delays," *Intern. Journal of Robotics Research*, vol. 23, no. 9, pp. 873–890, 2004.

[16] W. Ren, R. Beard, and E. Atkins, "Information consensus in multivehicle cooperative control," *IEEE Control Systems Magazine*, vol. 27, no. 2, pp. 71 –82, 2007.

[17] F. Bullo, J. Cortés, and S. Martínez, *Distributed Control of Robotic Networks*, ser. Applied Mathematics Series. Princeton University Press, 2009, electronically available at http://coordinationbook.info.